Carbohydrate Polymers 92 (2013) 726–732

Contents lists available at SciVerse ScienceDirect

Carbohydrate Polymers

journal homepage: www.elsevier.com/locate/carbpol

Dextran stabilized iron oxide nanoparticles: Synthesis, characterization and *in vitro* studies

Sheeja Liza Easo, P.V. Mohanan*

Division of Toxicology, Biomedical Technology Wing, Sree Chitra Tirunal Institute for Medical Sciences and Technology, Poojapura, Thiruvananthapuram 695012, Kerala, India

ARTICLE INFO

Article history:
Received 12 July 2012
Received in revised form 31 August 2012
Accepted 30 September 2012
Available online 8 October 2012

Keywords:
Iron oxide nanoparticles
Dextran
Co-precipitation
Superparamagnetism
Cytotoxicity

ABSTRACT

Iron oxide nanoparticles are one of the most important genres of nanoparticles with promise. Dextran, a stable biocompatible coating agent was employed in the synthesis of iron oxide nanoparticles in the presence of urea. The morphology of nanoparticles was confirmed by dynamic light scattering and transmission electron microscopy. These particles were also assessed for cytotoxicity, cellular uptake and cell adhesion *in vitro* using murine fibroblast cell line. The synthesized nanoparticles were superparamagnetic, possessed spherical shape with narrow size distribution and were found to be biocompatible and non-toxic. This study serves as a background for using DIONPs in further *in vitro* and *in vivo* studies with a long term goal of using it in biological applications.

© 2012 Elsevier Ltd. All rights reserved.

1. Introduction

Superparamagnetic iron oxide nanoparticles represent a class of materials with numerous potential applications in clinical and biomedical sciences such as MRI contrast enhancement, cellular therapy such as cell labeling and cell targeting, detoxification of biological fluids, hyperthermia, drug delivery and cell separation (Arbab et al., 2003; Häfeli, Schütt, Teller, & Zborowski, 1997; Pankhurst, Connolly, Jones, & Dobson, 2003; Reimer & Weissleder, 1996). These applications require nanoparticles to be of appropriate surface chemistry with high magnetization values, size smaller than 100 nm and narrow particle size distribution. In addition, magnetic particles also need to be non-toxic and biocompatible. The properties of magnetic nanoparticles are in turn, determined by several factors such as chemical composition, particle size and shape, interaction of the particle with the surrounding matrix and neighboring particles *etc*. A frequent problem with magnetic iron oxide nanoparticles is that due to their large surface area to volume ratio, they tend to aggregate in order to reduce their surface energy by forming strong magnetic dipole attractions between particles. Thus, the stabilization of superparamagnetic nanoparticles is essential to obtain magnetic colloidal ferrofluids that are stable against aggregation in both biological milieu as well as a magnetic field.

The main challenge in synthesizing magnetic nanoparticles involves obtaining monodisperse nanoparticles of suitable size and selecting a reproducible process without any complex purification procedure, such as ultracentrifugation, size-exclusion chromatography and magnetic filtration. A number of approaches have been described to produce magnetic nanoparticles which include microemulsions (Chin & Yaacob, 2007), sol–gel syntheses (Albornoz & Jacobo, 2005), sonochemical reactions (Kim, Lee, Kwak, & Kim, 2005), thermal reactions (Wan, Chen, Wang, Yang, & Qian, 2005), hydrolysis and thermolysis of precursors (Kimata, Nakagawa, & Hasegawa, 2003), flow injection syntheses (Alvarez, Muhammed, & Zagorodni, 2006) and electrospray syntheses (Basak, Chen, & Biswas, 2007). All these methods have been used to prepare particles with homogenous composition and narrow size distribution. However, the most common method for the production of iron oxide nanoparticles is the chemical precipitation of precursor iron salts (Lee, Jeong, Shin, Kim, & Kim, 2004; Martinez-Mera, Espinosa, Perez-Hernandez, & Arenas-Alatorre, 2007; Morrison, Cahill, Carpenter, Calvin, & Harris, 2005; Qiu, Yang, Li, & Jiang, 2005; Sun, Ma, Zhang, & Gu, 2004). The co-precipitation technique is probably the simplest and most efficient chemical route to obtain magnetic particles. The main advantage of the co-precipitation process is that a large amount of the particles can be synthesized easily and economically. Due to the tendency of magnetic nanoparticles to aggregate, it requires special surface coating which serves not only to make the particles non-toxic and biocompatible but also allows targeted delivery with particle localization in a specific area (Zhang, Kohler, & Zhang, 2002).

* Corresponding author. Tel.: +91 471 2520266.
E-mail address: mohanpv10@gmail.com (P.V. Mohanan).

0144-8617/$ – see front matter © 2012 Elsevier Ltd. All rights reserved.
http://dx.doi.org/10.1016/j.carbpol.2012.09.098

Several polymers have been investigated as coating agents such as dextran, carboxymethyl dextran, starch, polyethylene glycol (PEG), polyvinyl alcohol (PVA), polyoxamines, *etc.* (Lacava et al., 2001; Zhang et al., 2002). Among these, dextran has often been the choice of polymer coating because of its biocompatibility (Berry, Wells, Charles, & Curtis, 2003; Gamarra et al., 2005; Laurent et al., 2004). Dextran is a water soluble polysaccharide mainly composed of α-D-(1→6) linked glucose units and some α-D-(1→3) linked glucose branch units. In strongly alkaline solution, dextran interacts with hydroxyl groups present on iron oxide particles. Magnetite particles synthesized in the presence of dextran were shown to have prolonged blood residence time allowing access to macrophages located in tissues such as lymph nodes, kidney, brain, *etc.* (Molday & MacKenzie, 1982). Analysis of magnetic and structural properties of iron oxide synthesized in the presence of dextran suggests that the polymer limits particle size compared to uncoated particles (Pardoe, Chua-anusorn, St Pierre, & Dobson, 2001).

The physico-chemical characteristics of nanoparticles such as size, shape, surface charge and chemistry are important aspects in determining the blood circulation time of particles and their availability within the body. Particularly, it is the size of particles that decide the properties and biological fate of these particles (Chouly, Pouliquen, Lucet, Jeune, & Pellet, 1996). For instance, following systemic administration, particles greater than 200 nm are usually sequestered by spleen and eventually removed from circulation by cells of the phagocyte system, consequently decreasing their blood circulation times. Conversely, particles less than 10 nm in diameter are rapidly removed through extravasation and renal clearance. Particles in the range of 10–100 nm are small enough to elude both the reticuloendothelial system as well as to penetrate the very small capillaries within the body tissues and, hence may offer the most effective distribution in certain tissues (Stolnik, Illum, & Davis, 1995).

In this study, the co-precipitation method was modified in order to obtain uniform superparamagnetic iron oxide nanoparticles. Urea was used as an agent to manipulate the pH of the ferrite solution homogenously. The synthesized particles were characterized by various techniques. Furthermore, the effect of iron oxide particles on viability, adhesion capacity and morphology of L929 fibroblast cells has been assessed.

2. Materials and methods

2.1. Materials

All the chemicals used were of reagent grade without further purification. Ferric chloride hexahydrate ($FeCl_3{\cdot}6H_2O$), ferrous chloride tetrahydrate ($FeCl_2{\cdot}4H_2O$), formaldehyde, ammonium iron II sulphate, potassium permanganate, urea and hydrochloric acid (HCl) were purchased from Merck while dextran (MW 6000), tetramethylammonium hydroxide (TMAOH) solution 25 wt.% in water, 3-(4,5-dimethylthiazol-2-yl)-2,5-diphenyltetrazolium bromide (MTT), hydroxylamine hydrochloride, 1,10-phenenathroline monohydrate, minimum essential medium and antibiotic–antimycotic solution were obtained from Sigma. 0.25% trypsin–EDTA and fetal bovine serum were from Invitrogen.

2.2. Synthesis and coating of nanoparticles

Dextran stabilized iron oxide nanoparticles (DIONPs) were synthesized by *in situ* co-precipitation of ferrous and ferric salts with base TMAOH in the presence of urea in order to achieve homogenous precipitation. Briefly, $FeCl_2{\cdot}4H_2O$ and $FeCl_3{\cdot}6H_2O$ in a stoichiometric ratio of 1:2 was mixed with equal volume of urea and 2% dextran. The mixture was heated to 80–100 °C in order to decompose the urea. Subsequently, the reaction mixture was allowed to cool to room temperature and TMAOH was added drop-wise into the mixture. The entire reaction was carried out in nitrogen atmosphere with vigorous stirring. Formation of iron oxide nanoparticles was indicated by change in color of the solution from yellow to light brown to black. Large aggregates were removed by centrifugation and the remaining magnetic colloid was purified by dialysis against deionized water for 48 h with water changes twice daily. The resulting nanoparticles were found to be stable at 4 °C for over a period of six months during which no aggregation was observed. The iron content in DIONPs was determined as previously described (Mykhaylyk, Antequera, Vlaskou, & Plank, 2007).

2.3. Characterization of nanoparticles

The hydrodynamic size and size distribution of DIONPs was assessed by dynamic light scattering (DLS) instrument (Malvern Zetasizer, Nano ZS). Particle core size and morphology were examined using a transmission electron microscope (TEM) (Hitachi H-7650) at an accelerating voltage of 80 kV. The particles were analyzed for phase composition using X-ray diffraction (XRD) on a diffractometer (PANalytical X'Pert Pro MRD) using Cu-Kα radiation (λ = 1.54056 Å). Further, the thermal stability and content of polymer coating of DIONPs were checked by thermogravimetric analysis (TGA) (SDT-2960 TA). In order to confirm the iron oxide phase, the nature of coating and its bonding on the surface, Fourier transform infrared spectra (FTIR) was recorded between 4000 and 400 cm^{-1} at a resolution of 4 cm^{-1} on a Nicolet 5700 FTIR spectrometer. Finally, vibrating sample magnetometry (VSM) was used to measure the magnetic properties of DIONPs using a PAR EG&G Model 4500 magnetometer at room temperature.

2.4. In vitro studies

Cells seeded with 0.5 mg/mL DIONPs were visualized by Prussian blue staining for iron detection. The cells were washed thrice in phosphate buffered saline (PBS), pH 7.4 PBS, fixed with 4% buffered paraformaldehyde and incubated with 10% potassium ferrocyanide in 10% HCl for 30 min and washed again. Microscopic observation was done under bright light illumination (Axiostar plus, Carl Zeiss) and digital images were captured on a Canon PC 1200 camera.

To evaluate the cytotoxicity of DIONPs, L929 fibroblast cells were seeded at a density of 1×10^4 cells per well in a 96 well plate at 37 °C in 5% CO_2 atmosphere for 24 h. DIONPs at varying concentrations were added to cells and further incubated at 37 °C for another 24 h. Cells were then replenished with fresh media to allow them to recover from the effect of nanoparticle incubation. Subsequently, after 48 h of nanoparticle addition, 25 μL of MTT dye solution (2 mg/mL in PBS) was added to each well and incubated for 4 h. The insoluble formazan crystals were solubilized with 200 μL isopropanol and the solution was vigorously mixed to dissolve the crystals. After 30 min, the absorbance was read on a microplate reader (EL_x808 BioTek) at 540 nm. The spectrophotometer was calibrated to zero absorbance using culture medium without cells.

Fibroblast cells were expanded in culture, cells detached using trypsin–EDTA solution and used for cell adhesion assay. Cells were seeded with nanoparticles at concentration of 0.5 mg/mL for 24 h onto 13 mm coverslips at 37 °C in 5% CO_2 environment. Cells without nanoparticles were treated as control. The cells were washed twice with PBS, fixed in 4% buffered paraformaldehyde at 37 °C for 15 min and stained for 2 min in 1% Coomassie blue in acetic acid at room temperature. Stained cells in five random fields were counted using a light microscope (Axiostar plus, Zeiss) and the digital images were captured using a Canon PC 1200 camera. For evaluating cell

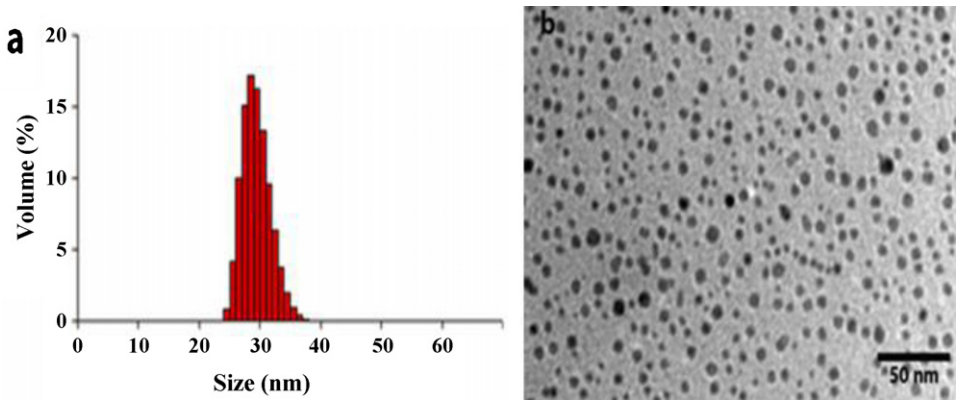

Fig. 1. Size characterization of DIONPs (a) hydrodynamic size profile as measured by dynamic light scattering shows a narrow size distribution with an average diameter of 25.3 ± 0.97 nm. (b) TEM image of the dextran stabilized iron oxide core indicates a spherical shape with mean size of 9.1 ± 1.46 nm.

surface morphology nanoparticle treated cells were fixed with 2.5% glutaraldehyde buffered in 1 M phosphate solution (pH 7.4) to allow viewing of individual cells. The fixed cells were examined on a environmental scanning electron microscope (ESEM) (Quanta 200 ESEM FEG, FEI) at a voltage of 12.50 kV.

3. Results and discussion

3.1. Mechanism of DIONPs formation

The co-precipitation process involves a short burst of nucleation followed by slow growth of the nuclei by diffusion of the solutes to the surface of the crystal (Boistelle & Astier, 1988; Cornell & Schwertmann, 1991, 1996; Gribanov, Bibik, Buzunov, & Naumov, 1990; Schwarzer & Peukert, 2004; Sugimoto, 2003). One aspect that is crucial to size control is the pH of the reaction mixture. It is well known that solutions of urea, when heated at 80 °C decomposes and produces ammonia (NH_3) while liberating hydroxide (OH^-) ions which can cause precipitation of metal oxide or hydroxide (Matijević & Hsu, 1987; Sordelet & Akinc, 1988; Wakefield, Holland, Dobson, & Hutchison, 2001). These hydroxide ions with the simultaneous addition of TMAOH help to homogenously elevate the pH of the system. It was also observed that the use of TMAOH facilitates continuous growth of the iron oxide crystals and also prevents secondary nucleation resulting in solution stability. Additionally, synthesis of iron oxide particles in an oxygen free environment prevents oxidation of iron oxide particles and also reduces their size (Kim, Zhang, Voit, Rap, & Muhammed, 2001).

Since nanoparticles have a large surface area to volume ratio, they tend to aggregate in order to reduce their surface energy. Nevertheless, colloidal suspensions of magnetic particles can be stabilized by coating the particles with high molecular weight polymers such as polyvinylalcohol (PVA), dextran, *etc.* and it has been suggested that such coatings are necessary for effective stabilization of ferrofluids (Zaitev, Filimonov, Presnyakov, Gambino, & Chu, 1999). Dextran was used to stabilize the particles because it enables maximum polar interactions with iron oxide surfaces. Although single hydrogen bonds in dextran are relatively weak, the large number of hydroxyl groups over the length of dextran molecules contributes substantially to the total bonding energy of hydrogen bonds (Tartaj, Morales, Veintemillas-Verdaguer, Gonzalez-Carreño, & Serna, 2006). While the mean size varied slightly between each preparation, the size distribution was always found to be less than 10% of standard deviation.

3.2. Characterization of DIONPS

The size distribution histogram of DIONPs shows that the mean hydrodynamic size of DIONPs was 25.3 ± 0.97 nm with narrow size distribution (Fig. 1a). TEM imaging of DIONPs indicate the particles to be spherical with an average core diameter of 9.12 ± 1.46 nm (Fig. 1b). In contrast to TEM measurements, DLS gave a significantly larger size for DIONPs. This is because the DLS method measures the hydrodynamic size in the dispersion medium, whereas TEM image gives the core particle size alone, without contribution from the dextran layer. XRD pattern of DIONPs indicates several distinct peaks at 30.1°, 35.6°, 43.1°, 57.2°, and 62.8°, accounting for crystal planes 200, 311, 400, 511, and 440 of spinel ferrite respectively (Fig. 2). The average crystalline size corresponding to the highest intensity peak (3 1 1) of the particles was calculated according to the Scherrer equation, $D = K\lambda/\beta\cos(\theta)$ where K is a constant equal to 0.94, λ is the X-ray wavelength, β is the full width at half maximum of the (3 1 1) peak expressed in radians, and θ is the Bragg angle corresponding to that peak. The average particle size obtained from

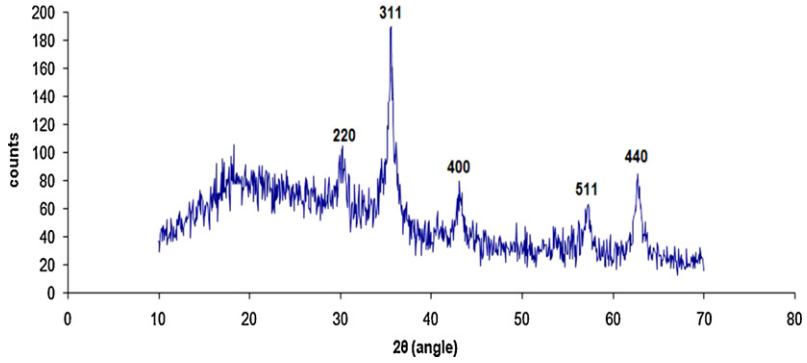

Fig. 2. X-ray diffraction pattern of dextran stabilized iron oxide particles can be indexed to reflections from the crystal planes of spinel ferrite.

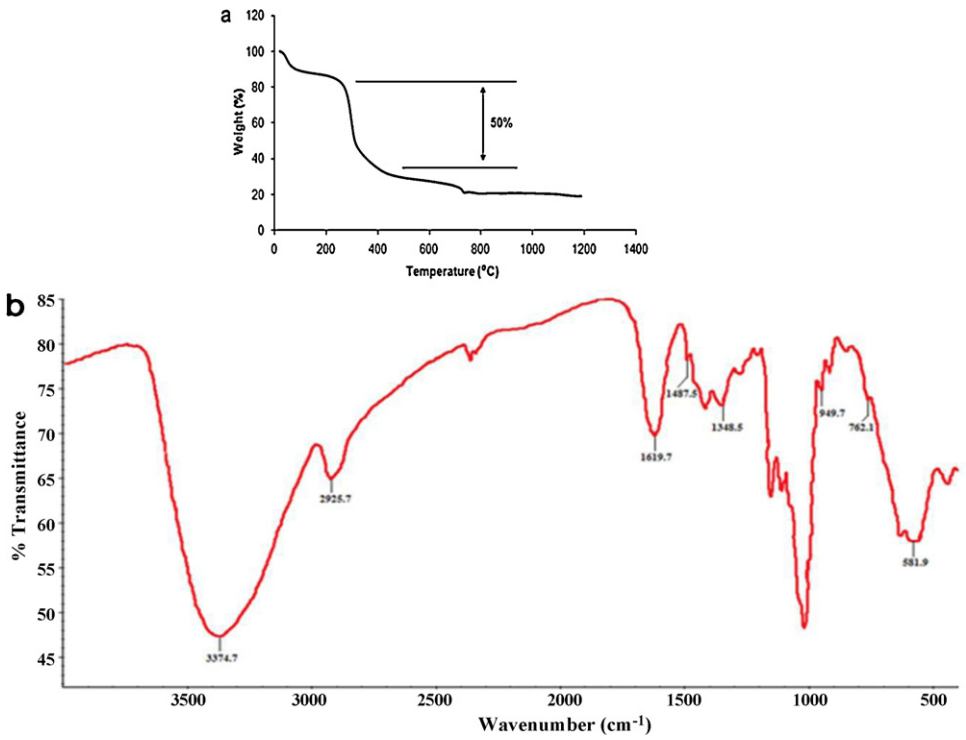

Fig. 3. (a) Thermogravimetric analysis data of dextran stabilized iron oxide nanoparticles. (b) Fourier transform infrared spectra of dextran stabilized iron oxide nanoparticles.

XRD data was found to be 8.69 nm. This value is close to the mean particle size observed from TEM.

In the thermal decomposition curve (Fig. 3a), the initial 6% weight loss in the range of 0–200 °C is due to physically adsorbed water. The next stage of decomposition corresponds to dextran breakdown and evolving. TGA data reveals remarkable weight loss largely above 200 °C implying that the polymer accounted for approximately 50 wt% of DIONPs. There is no significant weight change from 500 to 1000 °C indicating the presence of only iron oxide within the temperature range. According to the FTIR data, the peak at 3374.7 cm^{-1} is attributed to the stretching vibrations of —OH, which is assigned to OH^- absorbed by iron oxide nanoparticles and the peak at 581.9 cm^{-1} is attributed to the Fe—O bond vibration of iron oxide. The peak exhibited at 1619.7 cm^{-1} is attributed to water molecule bonding and peaks at 2925.7, 1487.5 and 1348.5 cm^{-1} are assigned to ν(C—H) and δ(C—H) vibrational modes and the peaks at 949.7 and 762.1 cm^{-1} due to α-glucopyranose ring deformation modes (Fig. 3b). Together these results confirm the presence of dextran coating on the iron oxide particles.

Fig. 4 shows the relative magnetization curve as a function of magnetic field for DIONPs. The absence of hysteresis curve indicates the characteristic superparamagnetic behavior of the particles. This superparamagnetic characteristic signifies that these particles have single domains and all magnetic moments are aligned in one direction. The saturation magnetization value of DIONPs was found to be 20.5 electromagnetic units per gram (emu/g). This low magnetization could be due to the dextran layer on the surface and stabilization of iron particles by TMAOH (Mørup, 1983; Si et al., 2005). For therapeutic purpose such as hypethermia, which is based on the power loss generated during heating of the nanoparticles, this limitation can be overcome by increasing the magnitude of the applied external AC magnetic field.

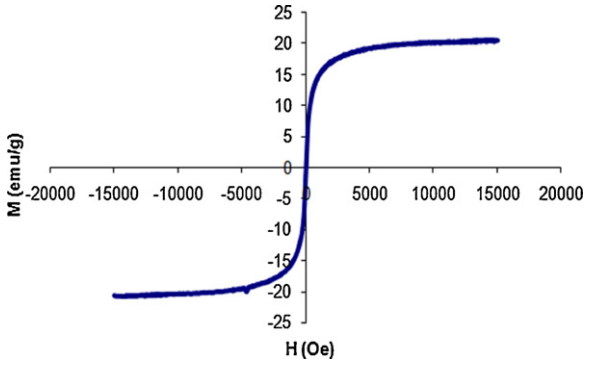

Fig. 4. Magetization curve of dextran stabilized iron oxide nanoparticles.

3.3. Cytotoxicity and cell adhesion assay

The MTT reduction assay is based on the mitochondrial metabolic activity of cells (Mosmann, 1993). Metabolically active cells reduce MTT into colored formazan crystals which can be determined spectrophotometrically. Although the particles affected cell

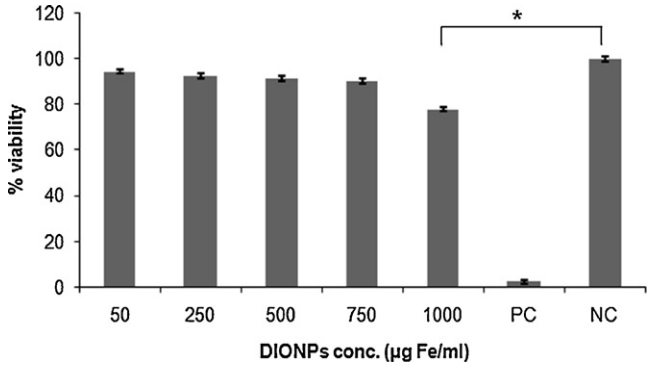

Fig. 5. Cytotoxicity profile of DIONPs when incubated with L929 cells. Percentage viability of fibroblast was expressed relative to control cells ($n = 6$). Results are represented as mean ± standard deviation. PC – positive control used 1% Triton X-100. NC – negative control. *Note*: * indicates statistical significant difference ($p < 0.05$).

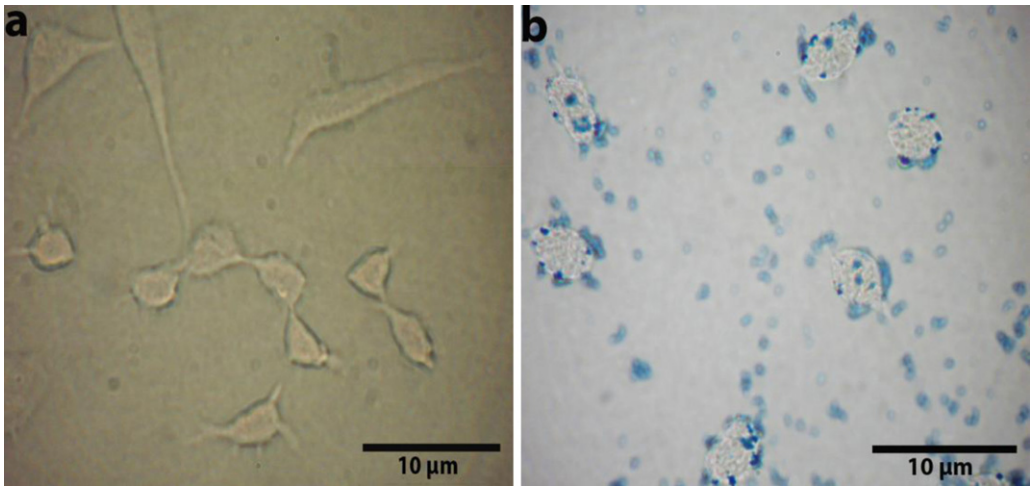

Fig. 6. Prussian blue staining (a) control and (b) cells incubated with DIONPs.

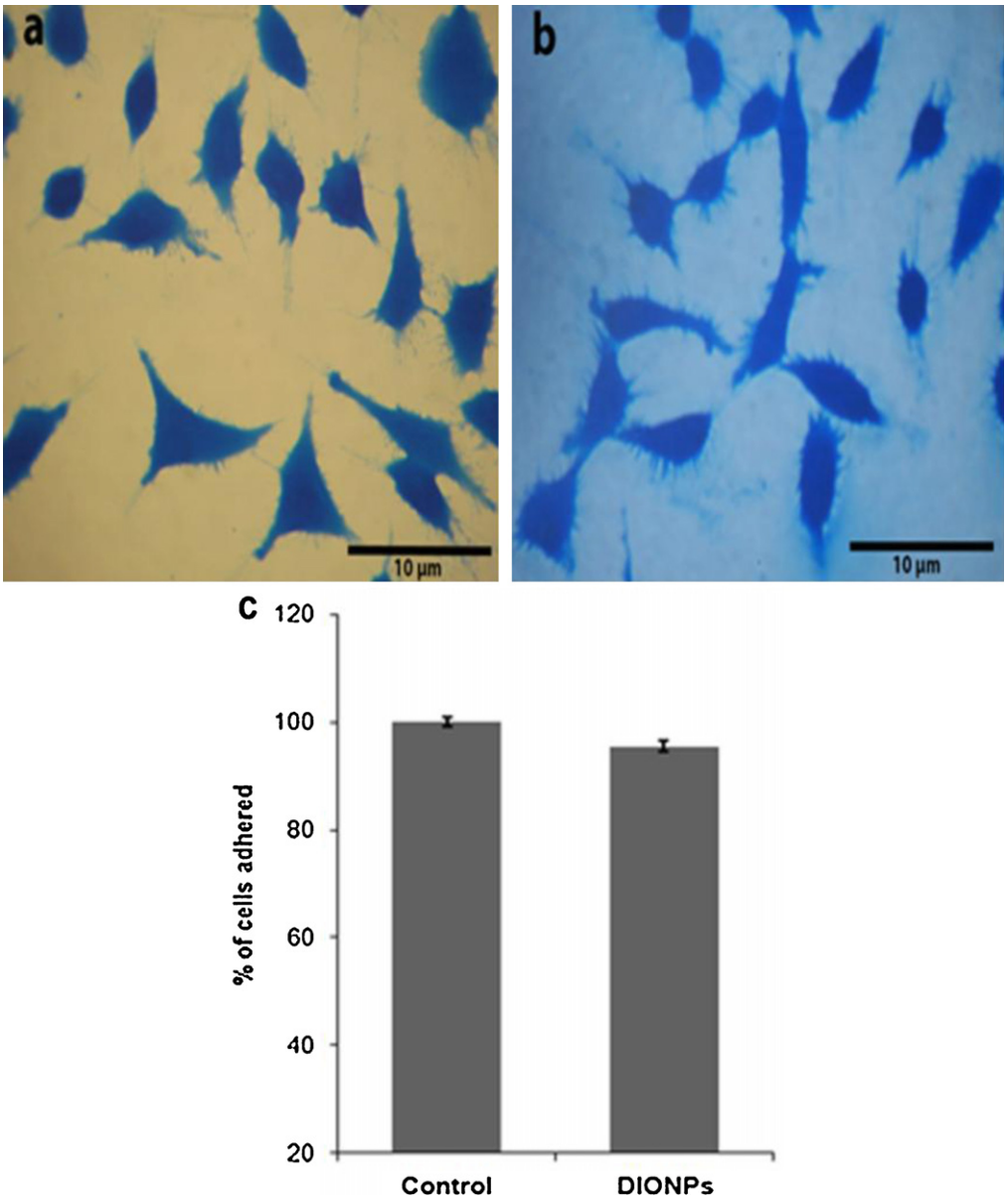

Fig. 7. Coomassie blue stained cells (a) control, (b) DIONPs, and (c) graphical representation of number of cells adhered when incubated with DIONPs ($n = 3$, counted in five different microscopic fields). Results are represented as mean ± standard deviation.

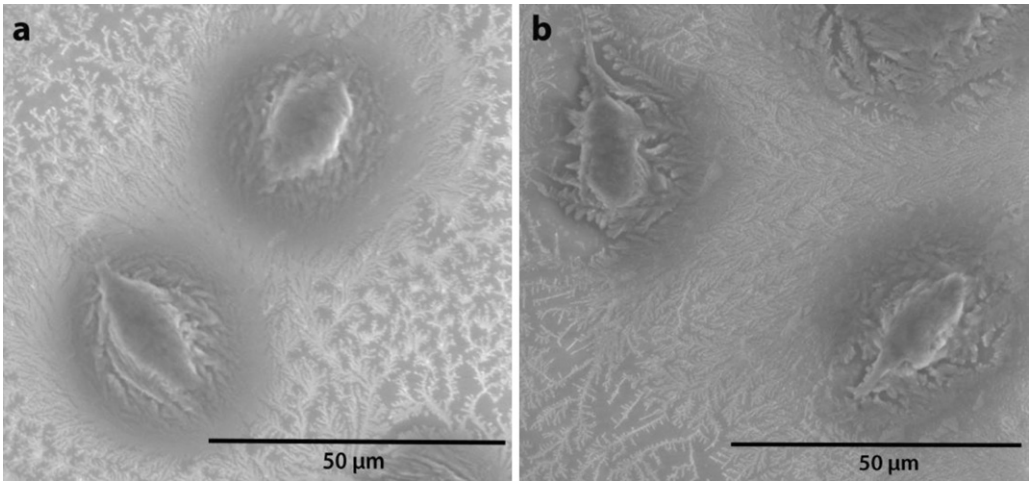

Fig. 8. ESEM image (a) control and (b) cells incubated with DIONPs.

viability in a concentration dependent manner, cells retained 90% viability relative to control at concentration as high as 0.75 mg/mL. But at the highest concentration tested (1 mg/mL) DIONPs caused a significant reduction in cell viability (Fig. 5). This reduction in cell viability in spite of the biocompatibility of dextran may be due to the breakdown of the dextran shell upon internalization resulting in particle chains and aggregates (Jordan et al., 1996). The effect of DIONPs on cell adhesion capacity of L929 cells was determined relative to control cells and it was observed that there was no significant decrease in the number of adhered cells grown in the presence of DIONPs (Fig. 6).

3.4. Prussian blue staining and analysis of cell morphology

After 24 h of incubation with DIONPs at a concentration of 0.5 mg/mL, nearly all cells were shown to contain iron indicating cellular uptake of DIONPs (Fig. 7). ESEM images of control cell population and cells treated with DIONPs revealed no distinct variation in cell morphology. The cells appeared to be flattened and well spread retaining their spindle shape and cell membrane integrity (Fig. 8).

4. Conclusion

Superparamagnetic DIONPs were prepared by modifying the co-precipitation method. Urea was used to homogenously alter the pH of the ferrite solution in the presence of TMAOH. The particles characterized by various techniques were found to have a narrow size distribution with phase composition similar to spinel ferrite. Coating of the particles with dextran was confirmed by TGA and FTIR studies. It was observed that DIONPs had negligible effect on cell adhesion capacity and morphology of L929 cells although cell viability was affected at the highest concentration of DIONPs tested. These preliminary *in vitro* studies implies that the synthesized DIONPs are biocompatible and provide a platform for using these particles in carrying out further *in vivo* investigations to assess its long term toxicity with the objective of developing iron oxide nanoparticles for biomedical applications.

Disclosure

The authors report no conflict of interest in this work.

Acknowledgements

The authors are grateful to the Director of Sree Chitra Tirunal Institute for Medical Sciences and Technology and Head of Biomedical Technology Wing for their support. The authors acknowledge the financial support provided by the Department of Science and Technology, India. The assistance of Dr. P.A. Joy, Physical and Materials Chemistry Division, National Chemical Laboratory, Pune in performing VSM studies and Mr. P. Guruswamy, National Institute for Disciplinary Science and Technology, Thiruvananthapuram, in conducting XRD experiments is kindly acknowledged. The service of Mr. Willie Paul and Mr. Praveen Kumar, Biosurface Technology Division in obtaining DLS measurements is appreciated. Sheeja Liza Easo acknowledges the Council of Scientific and Industrial Research (CSIR), New Delhi, India, for financial support.

References

Albornoz, C., & Jacobo, S. E. (2005). Preparation of a biocompatible magnetic film from an aqueous ferrofluid. *Journal of Magnetism and Magnetic Materials*, *305*, 12–15.

Alvarez, G. S., Muhammed, M., & Zagorodni, A. A. (2006). Novel flow injection synthesis of iron oxide nanoparticles with narrow size distribution. *Chemical Engineering Science*, *61*, 4625–4633.

Arbab, A. S., Bashaw, L. A., Miller, B. R., Jordan, E. K., Lewis, B. K., Kalish, H., & Frank, J. A. (2003). Characterization of biophysical and metabolic properties of cells labeled with superparamagnetic iron oxide nanoparticles and transfection agent for cellular MR imaging. *Radiology*, *229*, 838–846.

Basak, S., Chen, D. R., & Biswas, P. (2007). Electrospray of ionic precursor solutions to synthesize iron oxide nanoparticles: Modified scaling law. *Chemical Engineering Science*, *62*, 1263–1268.

Berry, C. C., Wells, S., Charles, S., & Curtis, A. S. G. (2003). Dextran and albumin derivatised iron oxide nanoparticles: Influence on fibroblasts in vitro. *Biomaterials*, *24*, 4551–4557.

Boistelle, R., & Astier, J. P. (1988). Crystallization mechanisms in solution. *Journal of Crystal Growth*, *90*, 14–30.

Chin, A. B., & Yaacob, I. I. (2007). Synthesis and characterization of magnetic iron oxide nanoparticles via w/o microemulsion and Massart's procedure. *Journal of Materials Processing Technology*, *191*, 235–237.

Chouly, C., Pouliquen, D., Lucet, I., Jeune, J. J., & Pellet, P. (1996). Development of superparamagnetic nanoparticles for MRI: Effect of particle size charge and surface nature on biodistribution. *Journal of Microencapsulation*, *13*, 245–255.

Cornell, R. M., & Schwertmann, U. (1991). *Iron oxides in the laboratory: Preparation and characterization* (1st ed.). Weinheim: Wiley-VCH Publishers.

Cornell, R. M., & Schwertmann, U. (1996). *The iron oxide* (1st ed.). Weinheim: Wiley-VCH Publishers.

Gamarra, L. F., Brito, G. E. S., Pontuschka, W. M., Amaro, E., Parma, A. H. C., & Goya, G. F. (2005). Biocompatible superparamagnetic iron oxide nanoparticles used for contrast agents: A structural and magnetic study. *Journal of Magnetism and Magnetic Materials*, *289*, 439–441.

Gribanov, N. M., Bibik, E. E., Buzunov, O. V., & Naumov, V. N. (1990). Physico-chemical regularities of obtaining highly dispersed magnetite by the method of chemical condensation. *Journal of Magnetism and Magnetic Materials*, *85*, 7–10.

Häfeli, U., Schütt, W., Teller, J., & Zborowski, M. (1997). *Scientific and clinical applications of magnetic carriers* (1st ed.). New York: Plenum Press.

Jordan, A., Wust, P., Scholz, R., Tesche, B., Fahling, H., Mitrovics, T., Vogl, T., Cervos-Navarro, J., & Felix, R. (1996). Cellular uptake of magnetic fluid particles and their effects on human carcinoma cell exposed to AC magnetic fields in vitro. *International Journal of Hyperthermia*, *12*, 705–722.

Kim, D. K., Zhang, Y., Voit, W., Rap, K. V., & Muhammed, M. (2001). Synthesis and characterization of surfactant coated superparamagnetic monodisperse iron oxide nanoparticles. *Journal of Magnetism and Magnetic Materials*, *225*, 30–36.

Kim, E. H., Lee, H. S., Kwak, B. K., & Kim, B. K. (2005). Synthesis of ferrofluid with magnetic nanoparticles by sonochemical method for MRI contrast agent. *Journal of Magnetism and Magnetic Materials*, *289*, 328–330.

Kimata, M., Nakagawa, D., & Hasegawa, M. (2003). Preparation of monodisperse magnetic particles by hydrolysis of iron alkoxide. *Powder Technology*, *132*, 112–118.

Lacava, L. M., Lacava, Z. G. M., Da Silva, M. F., Silva, O., Chavez, S. B., & Azevedo, R. B. (2001). Magnetic resonance of a dextran-coated magnetic fluid intravenously administered in mice. *Biophysical Journal*, *80*, 2483–2486.

Laurent, S., Nicotra, C., Gossuin, Y., Roch, A., Ouakssim, A., Vander Elst, L., Cornant, M., Soleil, P., & Muller, R. N. (2004). Influence of the length of the coating molecules on the nuclear magnetic relaxivity of superparamagnetic colloids. *Physica Status Solid*, *1*, 3644–3650.

Lee, S. J., Jeong, J. R., Shin, S. C., Kim, J. C., & Kim, J. D. (2004). Synthesis and characterization of superparamagnetic maghemite nanoparticles prepared by coprecipitation technique. *Journal of Magnetism and Magnetic Materials*, *282*, 147–150.

Martinez-Mera, I., Espinosa, M. E., Perez-Hernandez, R., & Arenas-Alatorre, J. (2007). Synthesis of magnetite (Fe_3O_4) nanoparticles without surfactants at room temperature. *Journal of Materials Science Letters*, *61*, 4447–4451.

Matijević, E., & Hsu, W. P. (1987). Preparation and properties of monodispersed colloidal particles of lanthanide compounds. I. Gadolinium, europium, terbium, samarium and cerium(III). *Journal of Colloid and Interface Science*, *118*, 506–523.

Molday, R. S., & MacKenzie, D. (1982). Immunospecific ferromagnetic iron-dextran reagents for the labeling and magnetic separation of cells. *Journal of Immunological Methods*, *52*, 353–367.

Morrison, S. A., Cahill, C. L., Carpenter, E. E., Calvin, S., & Harris, V. G. (2005). Atomic engineering of mixed ferrite and core–shell nanoparticles. *Journal of Nanoscience and Nanotechnology*, *5*, 1323–1344.

Mørup, S. (1983). Mössbauer spectroscopy studies of suspensions of Fe_3O_4 microcrystals. *Journal of Magnetism and Magnetic Materials*, *39*, 45–47.

Mosmann, T. (1993). Rapid colorimetric assay for cellular growth and survival: Application to proliferation and cytotoxic assay. *Journal of Immunological Methods*, *65*, 55–63.

Mykhaylyk, O., Antequera, Y. S., Vlaskou, D., & Plank, C. (2007). Generation of magnetic nonviral gene transfer agents and magnetofection in vitro. *Nature Protocols*, *2*, 2391–2411.

Pankhurst, Q. A., Connolly, J., Jones, S. K., & Dobson, J. (2003). Applications of magnetic nanoparticles in biomedicine. *Journal of Physics D: Applied Physics*, *36*, R167–R181.

Pardoe, H., Chua-anusorn, W., St Pierre, T. G., & Dobson, J. (2001). Structural and magnetic properties of nanscale iron oxide particles synthesized in the presence of dextran and polyvinyl alcohol. *Journal of Magnetism and Magnetic Materials*, *225*, 41–46.

Qiu, J., Yang, R., Li, M., & Jiang, N. (2005). Preparation and characterization of porous ultrafine Fe_2O_3 particles. *Materials Research Bulletin*, *40*, 1968–1975.

Reimer, P., & Weissleder, R. (1996). Development and experimental application of receptor-specific MR contrast media. *Radiology*, *36*, 153–163.

Schwarzer, H-C., & Peukert, W. (2004). Tailoring particle size through nanoparticle precipitation. *Chemical Engineering Communications*, *191*, 580–606.

Si, S. F., Li, C. H., Wang, X., Yu, D. P., Peng, Q., & Li, Y. D. (2005). Magnetic monodisperse Fe_3O_4 nanoparticles. *Crystal Growth and Design*, *5*, 391–393.

Sordelet, D., & Akinc, M. (1988). Preparation of spherical, monosized Y_2O_3 precursor particles. *Journal of Colloid and Interface Science*, *122*, 47–59.

Stolnik, S., Illum, L., & Davis, S. S. (1995). Long circulating microparticulate drug carriers. *Advanced Drug Delivery Reviews*, *16*, 195–214.

Sugimoto, T. (2003). Formation of monodispersed nano- and micro-particles controlled in size, shape and internal structure. *Chemical Engineering and Technology*, *26*, 313–321.

Sun, Y-K., Ma, M., Zhang, Y., & Gu, N. (2004). Synthesis of nanometer-size maghemite particles from magnetite. *Colloids and Surfaces A: Physicochemical and Engineering Aspects*, *245*, 15–19.

Tartaj, P., Morales, M. P., Veintemillas-Verdaguer, S., Gonzalez-Carreño, T., & Serna, C. J. (2006). Synthesis, properties and biomedical applications of magnetic nanoparticles. In K. H. J. Buschow (Ed.), *Handbook of magnetic materials*. Amsterdam, The Netherlands: Elsevier, pp. 403–482.

Wakefield, G., Holland, E., Dobson, P. J., & Hutchison, J. L. (2001). Luminescence properties of nanocrystalline Y_2O_3:Eu. *Advanced Materials*, *13*, 1557–1560.

Wan, J., Chen, X., Wang, Z., Yang, X., & Qian, Y. J. (2005). A soft-template-assisted hydrothermal approach to single-crystal Fe_3O_4 nanorods. *Journal of Crystal Growth*, *276*, 571–576.

Zaitev, V. S., Filimonov, D. S., Presnyakov, I. A., Gambino, R. J., & Chu, B. (1999). Physical and chemical properties of magnetite and magnetite-polymer nanoparticles and their colloidal dispersions. *Journal of Colloid and Interface Science*, *212*, 49–57.

Zhang, Y., Kohler, N., & Zhang, M. (2002). Surface modification of superparamagnetic magnetite nanoparticles and their intracellular uptake. *Biomaterials*, *23*, 1553–1561.